Jammed frictionless discs: connecting local and global response

Ellenbroek, W.G.; Hecke, M.L. van; Saarloos, W. van

Jammed frictionless disks: Connecting local and global response

Wouter G. Ellenbroek,[1,2] Martin van Hecke,[3] and Wim van Saarloos[1]
[1]*Instituut-Lorentz, Universiteit Leiden, Postbus 9506, 2300 RA Leiden, The Netherlands*
[2]*Department of Physics and Astronomy, University of Pennsylvania, Philadelphia, Pennsylvania 19104-6396, USA*
[3]*Kamerlingh Onnes Laboratory, Leiden University, P.O. Box 9504, 2300 RA Leiden, The Netherlands*
(Received 14 July 2009; revised manuscript received 13 October 2009; published 29 December 2009)

By calculating the linear response of packings of soft frictionless disks to quasistatic external perturbations, we investigate the critical scaling behavior of their elastic properties and nonaffine deformations as a function of the distance to jamming. Averaged over an ensemble of similar packings, these systems are well described by elasticity, while in single packings we determine a diverging length scale ℓ^* up to which the response of the system is dominated by the local packing disorder. This length scale, which we observe directly, diverges as $1/\Delta z$, where Δz is the difference between contact number and its isostatic value, and appears to scale identically to the length scale which had been introduced earlier in the interpretation of the spectrum of vibrational modes. It governs the crossover from isostatic behavior at the small scale to continuum behavior at the large scale; indeed we identify this length scale with the coarse graining length needed to obtain a smooth stress field. We characterize the nonaffine displacements of the particles using the *displacement angle distribution*, a local measure for the amount of relative sliding, and analyze the connection between local relative displacements and the elastic moduli.

DOI: 10.1103/PhysRevE.80.061307 PACS number(s): 45.70.−n, 46.65.+g, 83.80.Fg, 05.40.−a

I. INTRODUCTION

The jamming transition governs the onset of rigidity in disordered media as diverse as foams, colloidal suspensions, granular media, and glasses [1,2]. While jamming in these systems is controlled by a combination of density, shear stress, and temperature, most progress has been made for simple models of frictionless soft spheres that interact through purely repulsive contact forces that are at zero temperature and zero load [3–8]. This constitutes possibly the simplest model for jamming. Moreover, this is a suitable model for static foams or emulsions [9–11], which also represents a simplified version of granular media, ignoring friction [12–14] and nonspherical shapes [15–18].

From a theoretical point of view, this model is ideal for two reasons. First, it exhibits a well-defined jamming point, "point J," at confining pressure $p=0$, and in the limit of large system sizes, the jamming transition occurs for a well-defined density $\phi=\phi_c$, which has been identified with the random close packing density [3]. At this jamming point, the system is a disordered packing of frictionless undeformed spheres, which is marginally stable and isostatic, i.e., its contact number (average number of contacts per particle) z equals $z_{\mathrm{iso}}=2d$ in d dimensions. Second, in recent years it has been uncovered that the mechanical and geometric properties of such jammed packings of soft spheres close to point J exhibit a number of nontrivial power law scalings as a function of $\Delta\phi := \phi-\phi_c$. These scalings illustrate the unique character of the jamming transition [3–8].

Approaching point J from the jammed side, the most important scaling relations are as follows. (1) The excess contact number $\Delta z := z-z_{\mathrm{iso}}$ scales as $(\Delta\phi)^{1/2}$ [3,7,10,12]. (2) The ratio of shear (G) and bulk (K) elastic moduli vanishes at point J as $G/K\sim\Delta z$ [3]. (3) The density of vibrational modes exhibits a crossover from continuumlike behavior to a plateau at a characteristic frequency ω^*, which vanishes at the jamming point: $\omega^*\sim\Delta z$ [4,6,7]. One can associate a diverging length scale ℓ^* with this crossover, which then diverges at point J: $\ell^*\sim 1/\Delta z$ [6].

Recently, we uncovered an additional nontrivial scaling near point J when identifying the degree of nonaffinity [8]. Decomposing, for linear deformations of jammed systems, the relative displacement $\mathbf{u}_{ij}$ of neighboring particles i and j in components parallel ($u_\parallel$) and perpendicular ($u_\perp$) to $\mathbf{r}_{ij}$, where $\mathbf{r}_{ij}$ connects the centers of particles i and j, we find that the ratio $u_\perp/u_\parallel$ diverges near point J. More precisely, defining local displacement angles α_{ij} via $\tan\alpha_{ij}=u_{\perp,ij}/u_{\parallel,ij}$, we find that the displacement angle distribution $P(\alpha)$ peaks around $\alpha=\pi/2$, with the peak height diverging near point J. Hence, close to point J, the nonaffinity is such that particles predominantly *slide past* each other.

The nature of the nonaffinity of particle displacements ties in with the question to what extent these disordered solids close to the jamming transition can be described using continuum elasticity. Recent work on granular materials has shown that this is possible using the proper definitions of stress and strain tensor [19] and provided one probes the system at a large enough length scale [20–22]. However, it has remained unclear if this length scale is to be identified with the crossover length scale ℓ^* that was introduced in the interpretation of the density of vibrational states [6]. In addition, despite the large body of numerical and experimental work on the problem [23–29], a systematic analysis of the relations between the bulk elastic moduli, the stress fields in response to local perturbations, and the distance to the jamming transition appears to be lacking.

In this paper, we describe the applicability of elasticity theory for jammed packings and elaborate on our earlier work on the displacement angle distributions [8]. Although all our numerical studies are restricted to frictionless spheres in two dimensions, we expect essentially all concepts and conclusions to carry over to three dimensions.

In Sec. II we detail our linear response methodology and introduce our notation. In Sec. III we focus on the response

of jammed systems to local and global forcing and show that this response, suitably coarse grained and averaged, can be described by linear elasticity. Earlier direct numerical simulations [3,30] have established the scalings of the shear modulus G and bulk modulus K with distance to jamming and in particular have shown that their ratio G/K vanishes at point J. Our linear response calculations reproduce these findings.

In Sec. IV we address the issue of the length scale beyond which elasticity theory can be applied to the system. First, we determine this length directly from the response to a local perturbation, as the scale up to which the response is dominated by spatial fluctuations, and identify it with $\ell^* \sim 1/\Delta z$ [6]. In addition, we show that the coarse graining length, needed to obtain a smooth response in a globally deformed system, is proportional to the same length ℓ^*.

In Sec. V we characterize the nonaffine nature of the response to bulk deformations and elaborate on the scaling of the displacement angle distribution $P(\alpha)$. We discuss the connection between this scaling and the form of the expression for the changes in elastic energy in linear order: the opposite sign of the contribution from the parallel ($u_\parallel$) and perpendicular ($u_\perp$) components of the local displacements naturally leads to a delicate balancing act for the case of an overall shear deformation, while compression leads to a more convoluted picture [31].

II. LINEAR RESPONSE

All numerical results presented in this paper concern the quasistatic linear response of a certain starting configuration to a small perturbation. The approach is therefore explicitly a two-step one. First, we prepare a two-dimensional (2D) packing of frictionless polydisperse disks at a given density or confining pressure using a molecular dynamics (MD) simulation. The resulting packings are then analyzed by studying their response to small perturbations. Response studies have been done previously by using MD also for the perturbed system [30], in which case the full dynamics are taken into account. Another method that has been used is the quasistatic approach of minimizing the potential energy while ignoring inertia [3]. We here take the even simpler approach of explicitly focusing on the linear response equations. This requires solving just a single matrix equation for each numerical experiment, which makes it numerically cheap.

In the following sections we describe the procedure to generate our packings [13,32] and recapitulate the derivation of the linear response equation [8,33,34] from an expansion of the elastic energy of the system [7,35] both for completeness and to introduce the necessary notation.

A. Packing generation

We prepare our packings using a molecular dynamics simulation with round disks in two dimensions. The disks interact via the three-dimensional (3D) Hertzian potential,

$$V_{ij} = \begin{cases} \epsilon_{ij}\left(1 - \dfrac{r_{ij}}{d_{ij}}\right)^{5/2}, & r_{ij} \le d_{ij}, \\ 0, & r_{ij} \ge d_{ij}, \end{cases} \tag{1}$$

where i,j label the particles, d_{ij} is the sum of the particle radii R_i+R_j, and r_{ij} is the distance between the particle centers. The energy scale ϵ_{ij} depends on the radii and the effective Young moduli of the particles (see Appendix A). The quantity between parentheses is the dimensionless overlap, $\delta_{ij}=1-r_{ij}/d_{ij}$.

Using the 3D Hertzian potential makes the system a quasi-2D packing of disks with round edges. We use zero gravity to have a homogeneous pressure, and the radii of the disks are drawn from a flat distribution between $0.4<R<0.6$, thus creating a polydispersity of $\pm 20\%$ around the average particle diameter $d=1$ (our unit of length) to avoid crystallization. The simulation starts from a loose granular gas in a square box with periodic boundaries, which is compressed to a target pressure p by changing the radii of the particles while they are moving around. The radii are multiplied by a common scale factor r_s, which evolves in time via the damped equation $\ddot{r}_s = -4\omega_0 \dot{r}_s - \omega_0^2[p(t,r_s)/p - 1]r_s$, where $\omega_0 \sim 6\times 10^{-2}$, $p(t,r_s)$ is the instantaneous value of the pressure, and p is the target pressure. This ensures a very gentle equilibration of the packings. Energy is dissipated through inelastic collisions and a drag force which slows down the particles. The simulation stops when the accelerations of all grains have dropped below a threshold which is $10^{-6}\langle f\rangle$ in our reduced units. This way we generate packings in mechanical equilibrium for pressures ranging from $p=10^{-6}$ to $p=3\times 10^{-2}$ in units of the modified Young modulus of the individual grains [36]. This corresponds to a range of contact numbers from $z=4.05$ to $z=5.87$. For one particular type of calculation we use packings which are only periodic in the x direction and have hard walls on top and bottom. These are generated by compressing the system using a hard piston, as described in Ref. [32].

Because there is no gravity in our simulations, at the end of the simulation there will usually be particles without neighbors, or due to numerical precision effects, there will be particles with fewer neighbors than would be needed to make them rigidly connected to the rest of the packing. These *rattlers* or *floaters* do not contribute to the rigid backbone of the packing. They are removed from the system when determining the contact number z or calculating its linear response to small perturbations.

To express the distance to the jamming point, we will use the pressure p and typical relative overlap δ interchangeably; the pressure (rather than the density) is most conveniently set in the numerical procedure to generate the packings, while the overlap enters in the scaling relations at the particle scale that will be discussed in Sec. V. We do not use $\Delta\phi=\phi-\phi_c$ because in finite systems ϕ_c is a number that would have to be determined for each packing separately. However, close to point J we have determined that $\Delta\phi \sim \delta$. The conversion between the different parametrizations is given in Fig. 1.

B. Linear response equation

We calculate the response of a packing to a mechanical perturbation, which can be either an external force or a deformation of the periodic box. The response in general involves displacements of all particles in the packing, which we analyze in the linear regime.

The total potential energy of the system is a sum over all pairs of interacting particles,

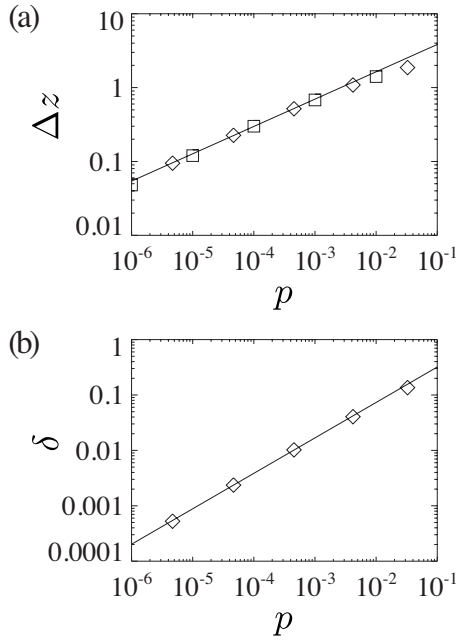

FIG. 1. The distance to the jamming transition is set in our packing preparation by the pressure p. Other parametrizations are (a) the distance to isostaticity $\Delta z = z - z_{\mathrm{iso}} \approx 9p^{0.37}$ and (b) the typical dimensionless interparticle overlap $\delta \approx 1.4p^{0.64}$. The solid lines represent these empirical power law fits. Diamonds represent periodic packings and squares are for packings with hard walls on top and bottom.

$$E = \sum_{\langle i,j \rangle} V_{ij}(r_{ij}), \tag{2}$$

where we assume we are dealing with a central potential, only depending on the distance between the particles $r_{ij} = |\mathbf{r}_{ij}| = |\mathbf{r}_j - \mathbf{r}_i|$. The change in r_{ij} due to displacements $\mathbf{u}_i$ of the particles is

$$\Delta r_{ij} = \sqrt{(r_{ij} + u_{\parallel,ij})^2 + u_{\perp,ij}^2} - r_{ij}, \tag{3}$$

where $u_\parallel$ is the relative displacement along the line connecting the centers of the particles and $u_\perp$ is the relative displacement perpendicular to that. In the linear response regime the change in energy is expanded to second order in $u_\parallel$ and $u_\perp$ as

$$\Delta E = \frac{1}{2} \sum_{\langle i,j \rangle} k_{ij} \left(u_{\parallel,ij}^2 - \frac{f_{ij}}{k_{ij} r_{ij}} u_{\perp,ij}^2 \right). \tag{4}$$

Here $f_{ij} = -dV_{ij}/dr_{ij}$ and $k_{ij} = d^2V_{ij}/dr_{ij}^2$. For all (power law) interactions that are reasonable models for foams or granular media (linear repulsion, Hertzian repulsion), both the initial force f and the stiffness k are non-negative (see below). There are no terms linear in the displacements because the starting configuration is in mechanical equilibrium, which makes these terms sum to zero. The $u_\parallel^2$ term represents the change in bond length. The $u_\perp^2$ term is only there if there is a prestress or initial force and captures the lowering of the energy due to transverse displacements of the particles [37].

The interaction potential for the particles that make up the packings used in this paper is a finite-range purely repulsive potential of the form $V \sim \delta_{ij}^\alpha$, where

$$\delta_{ij} = 1 - \frac{r_{ij}}{R_i + R_j} \tag{5}$$

is the dimensionless virtual overlap of the particles and R_i and R_j are the radii of particles i and j. The exponent α has the value $\alpha = 5/2$ in our packings, representing the three-dimensional Hertzian interaction. For any potential of power law form, the prefactor of the second term in Eq. (4) can be written as $\delta_{ij}/(\alpha - 1)$. The closer to point J, the smaller these dimensionless overlaps, so this prefactor will be small close to point J. However, this does not allow us to ignore this term because, as we will see, the typical $u_\perp$ is going to be much larger than the typical $u_\parallel$ in the limit of approaching the jamming transition: the two terms in Eq. (4) become, in some cases, of the same order.

Writing the change in energy in the independent variables of the problem, the displacements $\mathbf{u}_i$ of the particles, we define the dynamical matrix $\mathcal{M}$,

$$\Delta E = \frac{1}{2} \mathcal{M}_{ij,\alpha\beta} u_{i,\alpha} u_{j,\beta}, \tag{6}$$

where $\mathcal{M}$ is a $dN \times dN$ matrix (d being the spatial dimension and N being the number of particles). The indices α, β label the coordinate axes and we use the summation convention. The dynamical matrix contains all information on the elastic properties of the system. It can be diagonalized to study the vibrational properties [3,13,35], but it can also be used to study the response of the system to an external force (defined on each particle) [8,33,34],

$$\mathcal{M}_{ij,\alpha\beta} u_{j,\beta} = f_{i,\alpha}^{\mathrm{ext}}. \tag{7}$$

The dynamical matrix $\mathcal{M}$ is very sparse for large systems because the only nonzero elements are those for which i and j are in contact and those for which $i = j$. Therefore we can compute the response efficiently by using the conjugate gradient method [38]. This is essentially an iterative procedure that minimizes $\| \mathcal{M}_{ij,\alpha\beta} u_{j,\beta} - f_{i,\alpha}^{\mathrm{ext}} \|$. O'Hern *et al.* [3] also studied the quasistatic response of granular systems to a global shear or compression [3] using a conjugate gradient method, but in their case the quantity to be minimized was the potential energy. The difference is therefore that we use conjugate gradient only as an efficient method to study small deviations from a stable starting configuration in linear response, while O'Hern *et al.* used it for various situations where they needed to find the nearest potential energy minimum.

C. Forces and stresses

Solving the linear response equation [Eq. (7)] yields the displacements $\mathbf{u}_i$ of all particles. From this we calculate the local relative displacements $u_{\perp,ij}$ and $u_{\parallel,ij}$ and the change in contact force Δf_{ij} using

$$u_{\parallel,ij} = \cos \phi_{ij} u_{ij,x} + \sin \phi_{ij} u_{ij,y}, \tag{8}$$

$$u_{\perp,ij} = \cos \phi_{ij} u_{ij,y} - \sin \phi_{ij} u_{ij,x}, \tag{9}$$

$$\Delta f_{ij} = -ku_{\parallel,ij}, \tag{10}$$

where ϕ_{ij} is the angle which the bond vector $\mathbf{r}_{ij}$ makes with the x axis.

To get from discrete forces to a continuum stress field, we apply the local coarse graining procedure developed by Goldhirsch and Goldenberg [19],

$$\Delta\sigma_{\alpha\beta}(\mathbf{r}) = \sum_{\langle i,j\rangle} \Delta f_{ij,\alpha} r_{ij,\beta} \int_0^1 ds \Phi(\mathbf{r} - \mathbf{r}_j + s\mathbf{r}_{ij}). \tag{11}$$

It has been shown that this procedure gives local stress fields that do not depend strongly on the coarse graining length chosen—consistent results were obtained for length scales down to a single grain diameter [22]. In this paper, we use a Gaussian coarse graining function Φ with a width ξ_{CG} which is equal to the average particle diameter, $\xi_{CG}=1$ in our units, i.e.,

$$\Phi(\mathbf{r}) = \frac{1}{2\pi} e^{-|\mathbf{r}|^2/2}.$$

If, instead, one uses $\Phi = 1/V$, Eq. (11) reduces to the well-known expression for the average of the contact stress tensor over the entire system.

The precise form of Eq. (11) is not crucial for the work presented in this paper because we will only use this coarse graining procedure for the stresses and not for the strains. It is the requirement of emerging linear elasticity from coarse graining both stress and strain that led to this particular form in Ref. [19]. It should also be noted that, in principle, the expression for $\Delta\sigma$ contains both terms $\sim\Delta f r$ and $\sim f\Delta r$—we ignore the latter since these terms are negligibly small close to the jamming transition.

III. MACROSCOPICS AND CONTINUUM ELASTICITY

There are three questions that will be discussed here concerning the macroscopic aspects of the linear response of granular packings. First of all, under what conditions can the system's response to external forcing be described using continuum elasticity? Second, do we recover, in the linear regime, the scaling of the elastic moduli with contact number that was obtained in direct numerical simulations [3]? Finally, is there a difference in the values of the elastic moduli as calculated from the response to global forcing, using bulk compression or shear, and local forcing, applying an external force on a single particle?

The work by Goldenberg and Goldhirsch [19–22] has made clear that stress and strain tensors are well defined down to even less than the scale of a single grain using the coarse graining expressed by Eq. (11). For large enough systems, they find elasticity to provide a good description of the response of granular media. In this section, we analyze the response of granular packings *as a function of distance to the jamming transition* and confirm that the linear response of granular media, when averaged over an ensemble of similarly prepared packings, is well described by continuum elasticity. To do so, we study the response to both global and local perturbations, as described in Secs. III A and III B, respectively. A fit of the ensemble averaged stresses and displacements provides the elastic moduli of the packings, which we find to scale consistently with earlier results [3].

A. Bulk deformations

The conventional way to extract elastic constants of a packing is to apply a compression or shear deformation to the entire system. In packings with periodic boundaries this is done by imposing a relative displacement on all bonds that cross the boundary of the periodic box, following a procedure that is similar to the Lees-Edwards boundary conditions employed to simulate uniform shear flows [39]. For example, to impose a globally uniform compressional strain $\epsilon_{xx}=\epsilon_{yy}=\epsilon$, all terms in the energy expansion of Eq. (4) that represent a bond that crosses the periodic x boundary are changed such that each occurrence of $\mathbf{u}_j-\mathbf{u}_i$ is replaced by $\mathbf{u}_j-\mathbf{u}_i\pm\epsilon L_x\hat{\mathbf{x}}$, where the $\pm$ sign is given by the sign of $r_{ij,x}$. The y boundary is treated analogously. Shear deformations are applied in the form of a pure shear, i.e., by having a displacement in the y direction imposed on all bonds that cross the x boundary *and* a displacement in the x direction on all bonds that cross the y boundary.

When we write the linear response equation [Eq. (7)] from the energy expression for the deformed system, the terms proportional to ϵ end up on the right-hand side of the equation and act like an effective f^{ext}. The response of the system to this shape or volume change of the periodic box is again calculated by solving Eq. (7) for this effective external force. The elastic moduli then follow from the resulting change in stress tensor according to Eq. (11) with the trivial coarse graining function $\Phi=1/V$. The bulk modulus is extracted from a uniform compressional strain $\epsilon_{xx}=\epsilon_{yy}=\epsilon$ through

$$K = \frac{\sigma_{\alpha\alpha}}{2\epsilon_{\alpha\alpha}} = \frac{\sigma_{xx}+\sigma_{yy}}{4\epsilon} \tag{12}$$

and the shear modulus from a uniform shear strain $\epsilon_{xy}=\epsilon$ through

$$G = \frac{\sigma_{xy}}{2\epsilon_{xy}} = \frac{\sigma_{xy}}{2\epsilon}. \tag{13}$$

The results will be presented and discussed in Sec. III C together with those obtained from the local point response.

B. Point response

Now let us determine the linear response of packings of $N=10\,000$ particles to a force in the y direction, applied to a single particle. The packings are periodic in the x direction and have hard walls on top and bottom to carry the load. The confining pressure p used to create the packings ranges from $p=10^{-6}$ to $p=10^{-2}$, corresponding to contact numbers ranging from $z=4.05$ to $z=5.41$. We have ten different packings at each pressure and use each one about 20 times by applying a point force to different particles, all of which are closer than 0.1 particle diameter to the horizontal line through the center of the system. Examples of the resulting *response networks*, depicting the changes in the contact forces, are shown

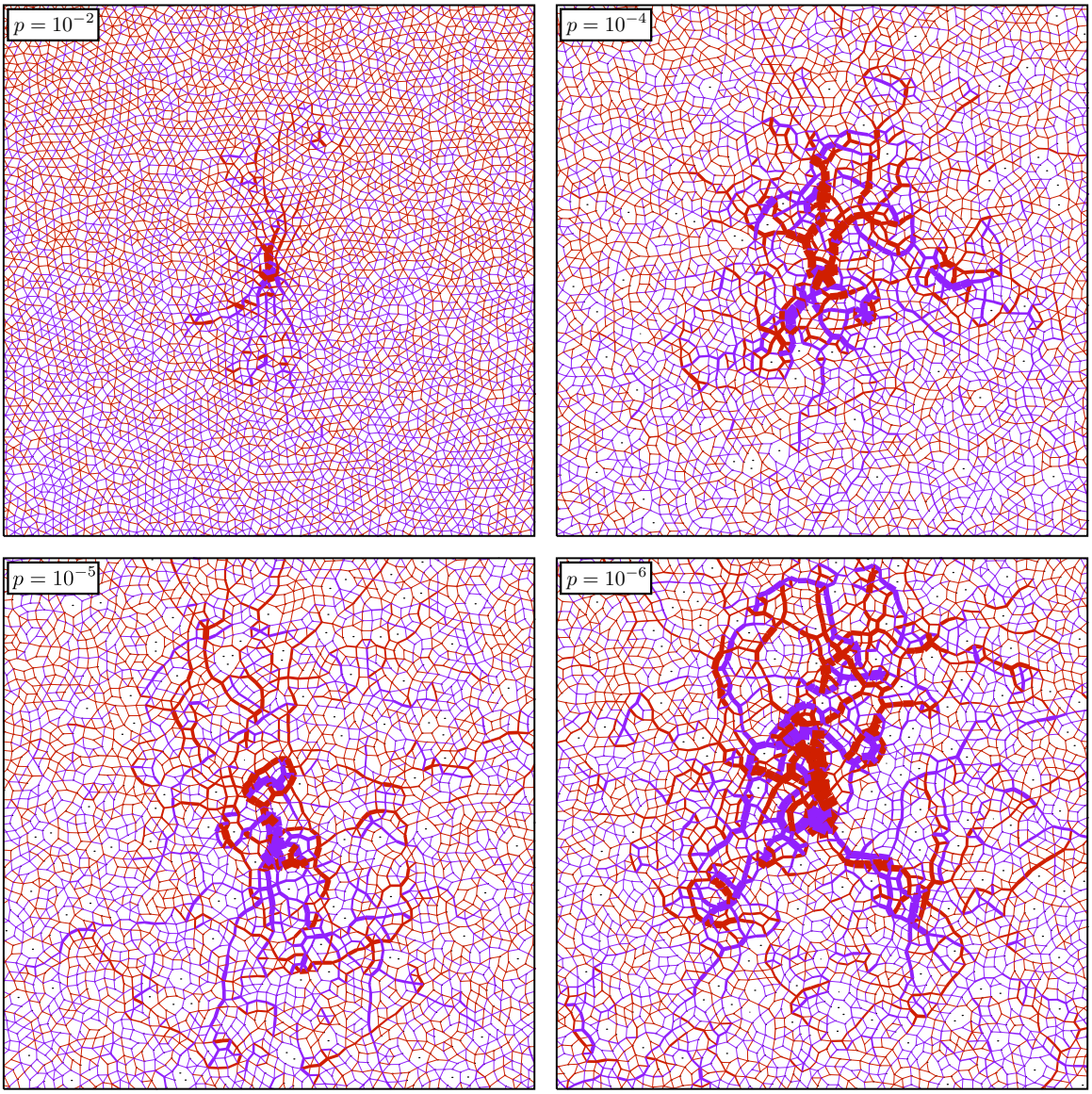

FIG. 2. (Color online) Force response networks for a point loading with pressure as indicated. Blue (red) lines indicate an increase (decrease) of the contact force, the thickness indicating the amount (the thickness of the black border around each panel corresponds to 1/15 of the loading force on the center particle). The particles themselves are not drawn. The figures show only the central part (size 56×56) of the packing close to the forced grain and contain about 3500 of the 10 000 particles. Note that in the black and white print, the blue lines will show up darker than the red lines.

in Fig. 2. These pictures immediately illustrate to the eyes that as the jamming point is approached, both the range and the magnitude of the fluctuations increase. Quantifying this behavior is the goal of Sec. IV—here we focus first on the ensemble averaged response.

In order to allow comparison to continuum solutions, we first calculate for each force response network the associated stress response fields by the coarse graining procedure in Eq. (11) (see Ref. [19] for details). We then calculate the ensemble average of these stress response fields, and results of this procedure are shown in Fig. 3. The continuum solution that we are comparing the granular point response to is obtained from the static Navier-Cauchy equation [40], which is given by

$$G\Delta\mathbf{u} + K\nabla(\nabla\cdot\mathbf{u}) = -\mathbf{f}^{\text{ext}} \tag{14}$$

in a two-dimensional formulation of elasticity theory. Here K and G denote bulk and shear moduli. This equation is the direct equivalent of the linear response equation [Eq. (7)] because solving it yields displacements in terms of external forces. We solve Eq. (14) with $\mathbf{f}^{\text{ext}}$ equal to a unit point force in the y direction (see Appendix B for details). The resulting stress field $\sigma_{\alpha\beta}(\mathbf{r})$ only depends on the ratio K/G of elastic constants since the overall scale drops out when relating an imposed force to a resulting stress. Therefore, there is only one free parameter when fitting the stress field of the granular system [Eq. (11)] to the continuum expression. As described in Appendix B, we use the effective Poisson ratio ν

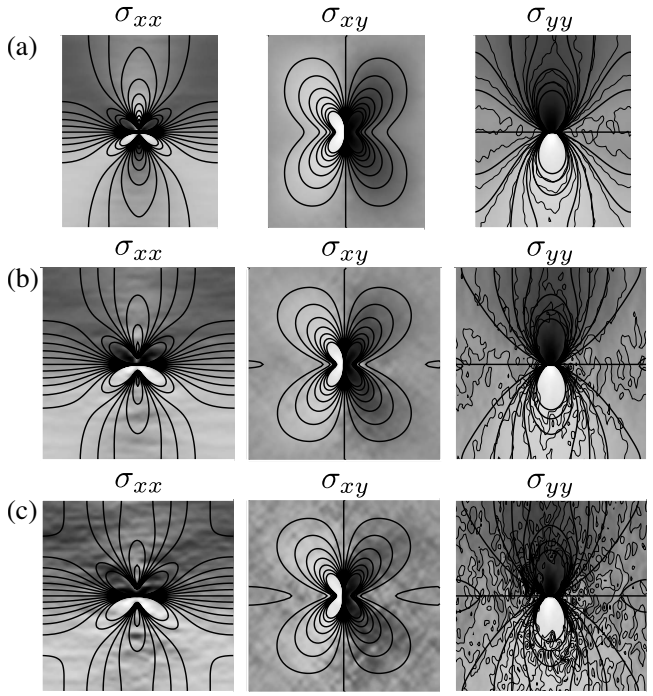

FIG. 3. Stress response fields for the linear response to a point force. The grayscale images represent the ensemble averaged granular stress response field; the thick contours denote the fitted continuum stress field. For σ_{yy} thin contours for the granular stress response field are included as well. The components of the stress tensor are plotted for (a) $p=10^{-2}$, (b) $p=10^{-4}$, and (c) $p=10^{-6}$.

$=(K-G)/(K+G)$. To determine both moduli we need a second fitting parameter using a fit to the displacement field. In particular, we fit the average y displacement of all particles in a strip at height y,

$$H_{\text{gran}}(y) := \langle u_{i,y} \rangle_{y_i \approx y}, \tag{15}$$

to its continuum counterpart,

$$H(y) := \frac{1}{L_x} \int_{-L_x/2}^{L_x/2} u_y(x,y)dx = \frac{L_y - 2|y|}{4L_x(K+G)}, \tag{16}$$

which is obtained by taking $\mathbf{f}^{\text{ext}} = \delta(x)\delta(y)\hat{\mathbf{y}}$ and integrating Eq. (14) over x, leaving a standard Green's function problem with the boundary condition that u_y vanishes at the top and bottom walls, i.e., at $y = \pm L_y/2$.

Figure 3 displays the ensemble averaged stress response fields $\Delta\sigma_{\alpha\beta}(\mathbf{r})$ [Eq. (11)] and the fitted continuum stress fields for $p=10^{-2}$, $p=10^{-4}$, and $p=10^{-6}$. The gray scale and the contour values are chosen for each tensor component separately, but for each component they are the same for the different pressures. The fit is very good, especially considering the fact that a tensor field with three components is fitted with only one parameter. For the yy component we also include contours for the numerical data to give a more quantitative view of the fit. For the xx and xy components the numerical data are too noisy for this to be useful, especially at the lower pressures.

The fits of the average vertical displacements $H_{\text{gran}}(y)$ are shown in Fig. 4. Again a good fit is obtained with only one parameter, with only a little bit of noise for the lowest pressure packings. Combining the results of the two fitting procedures yields the elastic moduli—the results are presented in Sec. III C.

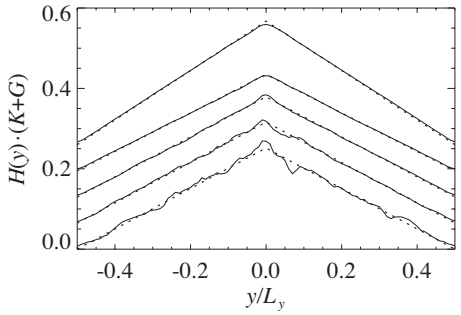

FIG. 4. The fitting procedure used to obtain $K+G$: the average vertical displacement of particles at height y [Eq. (15)] is fitted to the triangle-shaped function $H(y)$ given by Eq. (16). The functions are rescaled by the fitted $K+G$ and vertically offset for clarity [note that $H(y)=0$ for $y/L_y = \pm\frac{1}{2}$].

C. Results

The elastic moduli resulting from the methods explained in Secs. III A and III B are collected in Fig. 5(a). The squares and diamonds represent the bulk (K) and shear (G) moduli, respectively, calculated from the linear response to a bulk compression or shear. These have been obtained via ensemble averages over 100 packings of $N=1000$ particles for pressures ranging from $p=5\times10^{-6}$ to $p=3\times10^{-2}$ (in units of the modified Young modulus of the grains). This pressure range corresponds to a range in contact number from $z=4.10$ to $z=5.87$. The cross and plus signs indicate the moduli resulting from fitting the stress response to a point force to continuum elasticity. As mentioned in Sec. III B, the packings used for the point response calculations were prepared at pressures ranging from $p=10^{-6}$ to $p=10^{-2}$, corresponding to contact numbers from $z=4.05$ to $z=5.41$.

From Fig. 5 one sees that the data are well described [54] by scaling relations of the form

$$K \sim p^{0.36\pm0.03}, \tag{17}$$

$$G \sim p^{0.70\pm0.08}. \tag{18}$$

These are consistent with the scalings $K\sim p^{1/3}$ and $G\sim p^{2/3}$ which on the basis of previous work [3] are expected for our 3D Hertzian contacts. The above scaling behavior already shows that we can consistently describe the response in terms of continuum elasticity.

Alternatively, we can plot the ratio of the elastic moduli as a function of Δz and find that G/K scales as Δz [Fig. 5(b)]. This result is expected to be independent of the force law—in all disordered packings that have been checked, the bulk modulus K is proportional to the contact stiffness k, while the shear modulus G behaves proportional to $k\Delta z$ [3,30,41]. The scaling of the shear modulus has been described as anomalous [3,12,30] because earlier *effective medium theories* had predicted $K\sim G\sim k$ [12,42]. However,

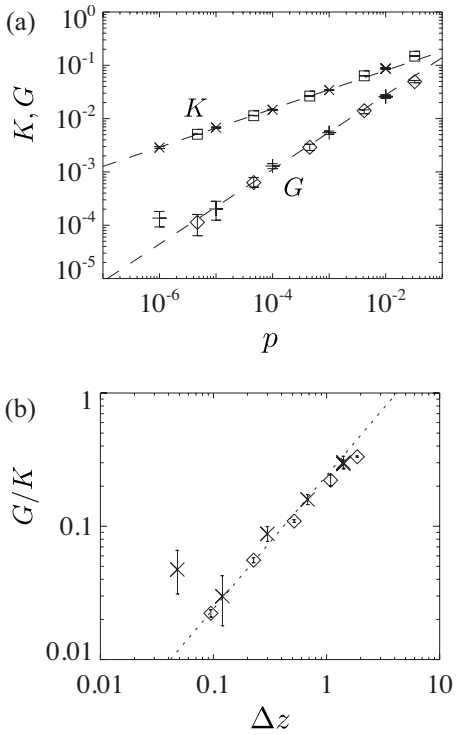

FIG. 5. (a) Bulk modulus K and shear modulus G as a function of pressure. The squares (K) and diamonds (G) are obtained using the bulk response described in Sec. III A. The crosses (K) and plus signs (G) follow from the fits of the point response stresses and displacements discussed in Sec. III B. The error bars on the bulk response data indicate the intervals spanned by the median 50% of the data; the actual standard error of the mean is much smaller than the symbol size. The error bars on the point response data are error estimates from the fitting procedure. We attribute the fact that the point response result for G at the smallest pressure deviates from the scaling behavior to the fact that our fitting to elastic continuum behavior is very insensitive to the value of G in the limit $G \ll K$. (b) The ratio of elastic moduli G/K scales approximately as Δz.

from the perspective of rigidity percolation on a random network, for which all elastic moduli are proportional to Δz, the compression modulus can be described as anomalous. We have recently explored this issue extensively in the context of harmonic networks [31].

Our calculations show that the average large scale response to both a local force and a global deformation or force is consistent with continuum elasticity theory with the *same* elastic moduli. We thus conclude that the linear response to a local perturbation, *averaged* over an ensemble of packings, is well described by linear elasticity. To what extent and on what length scale the response of a *single* packing corresponds to elastic behavior will be the subject of Sec. IV.

Let us close this section by pointing out the effect of the second term in the energy expansion [Eq. (4)], which is proportional to $u_\perp^2$. This term contains the influence of the forces that the contacts carry before applying the external point force and is therefore referred to as the *prestress* term [37]. This term is strictly negative in a system of purely repulsive particles and therefore tends to destabilize the system to enhance the perpendicular (sliding) motions of particles and to lower the energy associated with deformations. To study its effect, we also performed a calculation in which we left it out. The destabilization can be seen from comparing Fig. 6(a) with Fig. 6(b): the spatial fluctuations from the continuum elasticity stress fields are much smaller if we leave out the prestress term. The fact that the elastic energies are lower when the term $\propto u_\perp^2$ is included in the energy expansion can also be shown by calculating the elastic moduli with and without this prestress term. The resulting shear modulus without this term is higher than when this term is included. We will come back to the relative importance of the two terms in the energy expansion in Sec. V.

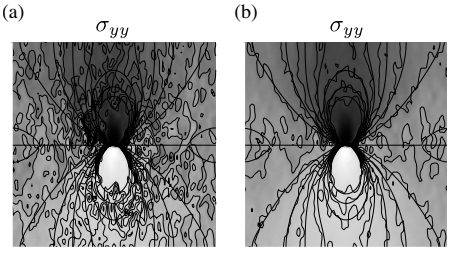

FIG. 6. Comparison of the stress response to a point force of a packing close to the jamming transition ($p=10^{-6}$) (a) calculated with the energy expansion as stated in Eq. (4) and (b) calculated without the $u_\perp^2$ term, which corresponds to ignoring the forces present in the system before the point force was applied. Thick curves are the continuum fit and thin curves are the numerical contours as in Fig. 3.

IV. CRITICAL LENGTH SCALE

In Sec. III C we have seen that the ensemble averaged response of a jammed granular medium can be described using continuum elasticity. On the other hand, the disordered nature of the packing has a strong effect on the displacements and forces in individual realizations, especially in systems close to the jamming transition. The question is whether we can think about the role of disorder as relevant on small length scales but sufficiently smeared out on long length scales. We will probe this question by locally forcing the system and studying the fluctuations away from the ensemble averaged response as a function of length scale. We will find a length scale ℓ^* which indicates above what length one can consider the system a continuum medium. This length scale is proportional to $1/\Delta z$, which implies that it diverges as we approach the jamming transition.

The length scale ℓ^* was introduced earlier by Wyart *et al.* to describe the excess of low frequency modes in the density of vibrational states of these systems [6], where it can be derived as follows. If a system of dimension d is to be described as a continuum medium, it should keep its properties when cut open and split in two parts. In particular, if we cut out a circular blob of radius ℓ of a rigid material, it should remain rigid. The rigidity (given by the shear modulus) of jammed granular materials is proportional to Δz, the density of excess contacts over the minimum number of contacts required to be mechanically stable. The circular blob has of

the order $\ell^d \Delta z$ of such contacts. To cut it out, however, we had to break the contacts at the perimeter of which there are of order $z\ell^{d-1}$. If the number of broken contacts at the edge is larger than the number of excess contacts in the bulk, the resulting blob is not rigid but floppy (see Appendix C). The smallest blob one can cut out without it being floppy is obtained when these numbers are equal, which implies that it has radius $\ell^* \sim z/\Delta z$. Close to the jamming transition, z is essentially constant, and so one obtains as scaling relation that [7]

$$\ell^* \sim \frac{1}{\Delta z}. \tag{19}$$

So far this length scale ℓ^* has not been observed directly. What has been observed is a crossover frequency ω^* in the density of vibrational states, marking the lower end of a plateau of excess states. The vibrational states at $\omega < \omega^*$ have been interpreted as ordinary plane-wave-like modes [4,6]. Using the speed of sound one can therefore translate the crossover frequency into a wavelength, which scales as $\lambda_T \sim 1/\sqrt{\Delta z}$ for transverse (shear) waves and as $\lambda_L \sim 1/\Delta z$ for longitudinal (compressional) waves. λ_T has been observed in the spatial structure of the vibrational modes by Silbert *et al.* [4], but it is λ_L that coincides with the length scale ℓ^* derived above. Note that the derivation of ℓ^* involved neither shear nor compression waves and therefore the correspondence of ℓ^* and λ_L is not obvious *a priori*. Below we present the real-space observation of ℓ^* in the fluctuations of the force response to a localized perturbation.

A. Observation of ℓ^* in inflation response

The signature of the length scale ℓ^* can readily be observed in the point force response networks (see Fig. 2): the lower the pressure and hence the smaller Δz, the larger the scale up to which the response looks disordered. To study this effect quantitatively, we calculate the response to an inflation of a single central particle (Fig. 7) instead of directional point forcing (Fig. 2). This allows us to probe a natural length scale of the system, as we expect a crossover between the behavior for small and large r: far away from the inflated particle we expect a smooth response with radial symmetry, for which $\Delta\sigma_{rr}$ [55],

$$\Delta\sigma_{rr} \approx \frac{G}{r^2},$$

while nearby, the disorder dominates the response. As we will show now, the crossover length can be identified with ℓ^*.

Examples of the changes in contact forces Δf in response to the inflation of a single particle are shown in Fig. 7 for pressures $p = 4 \times 10^{-3}$ and $p = 5 \times 10^{-5}$. For a fixed change in radius of the central particle, the scale of Δf is strongly influenced by the stiffness of the few contacts of this particle, leading to large fluctuations in the amplitude of Δf. Since we are mainly interested in the spatial structure rather than the values of Δf, we first normalize the force response Δf. To do so, we fit the change of each local radial stress $\Delta\sigma_{rr}$ to the

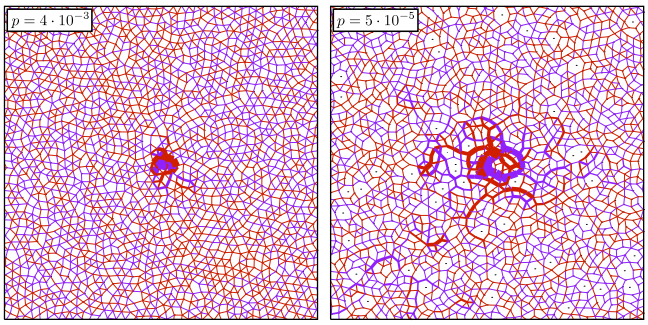

FIG. 7. (Color online) Force response networks for inflation of a single particle, with p as indicated. Blue (red) lines indicate positive (negative) changes in contact force, the thickness indicating the amount, which is drawn for a 2% increase of the particle diameter. The thickness of the border around the panel corresponds to a change in force of 1/4500 (left) and 1/60 000 (right), respectively, which is needed because the shear modulus is much lower at the lower pressure. The particles themselves are not drawn. The figures show only the part of the packing close to the inflated grain (size 42×42) and contain about 1800 of the 10 000 particles. Note that in the black and white print, the blue lines will show up darker than the red lines.

continuum field (with a correction for the periodic boundaries),

$$\Delta\sigma_{rr} \approx \frac{G_{\mathrm{fit}}}{r^2},$$

and define the normalized response Δf^{n} as $\Delta f / G_{\mathrm{fit}}$. In exceptional cases, the fitting parameter G_{fit} is anomalously small. Inspection of the response networks in which this happens reveals relatively large "soft spots," regions where the rearrangements of the particles are large. We leave an analysis of these soft spots and their relevance to the future; for the present analysis we limit ourselves to noting that these soft spots sometimes lead to very bad fits of the stress field and discard the 1% worst-fitting response networks.

In view of the radial symmetry, on average, we study the fluctuations in the response at a distance r from the inflated grain. More precisely, we calculate the root mean square fluctuations of the radial component of the normalized force response, Δf_r^{n}, through all contacts at that particular distance r,

$$h(r) \equiv \sqrt{\langle [\Delta f_r^{\mathrm{n}}(r) - \langle \Delta f_r^{\mathrm{n}}(r) \rangle]^2 \rangle}. \tag{20}$$

Here the average $\langle \cdot \rangle$ is taken over all bonds that intersect the circle of radius r centered around the inflated particle. Note that $h(r)$ is not a simple correlation function in the ordinary sense: it simultaneously involves *all* contacts at a distance r from the center and cannot be expressed in terms of a single n-point correlation function. We calculate this function for packings of $N = 10\,000$ particles and average over 356 response networks at each value of p. The resulting $h(r)$ are shown in Fig. 8(a). As expected, the fluctuations are larger and longer ranged for packings at smaller pressure. Figure 8(b) shows the decay on a double logarithmic plot: it appears that for large r the tail of $h(r)$ goes roughly as $1/r^{1.6}$ while

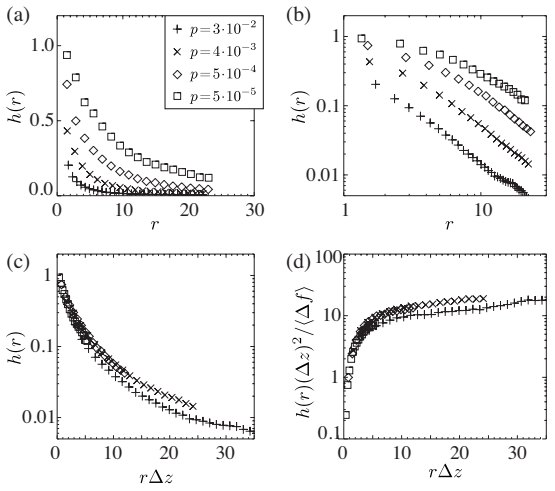

FIG. 8. Identification of the length scale ℓ^*. (a) The fluctuations in the contact forces, measured by $h(r)$, which is defined in Eq. (20), are larger in the response of packings at low pressure. (b) The same data on a double logarithmic plot shows that the tail decays as a power law approximately as $1/r^{1.6}$. (c) The data collapse when we rescale the r axis by Δz, signaling a length scale that scales as $\ell^* \sim 1/\Delta z$. (d) The relative fluctuations (fluctuations divided by the average value of the contact forces).

the small r behavior has a smaller slope that varies with p. The crossover scale between these regimes is proportional to the length scale ℓ^*, as is illustrated by the data collapse that is obtained when $h(r)$ is plotted as a function of $r\Delta z$ in Fig. 8(c). One might expect the fluctuations to decay as r^{-2}, following the decay of the stress. We attribute the difference in exponent to finite size effects.

In Fig. 8(d) we plot the *relative* fluctuations with respect to the average radially transmitted force $\langle \Delta f_r^n(r)\rangle$ [Fig. 8(d)]. These are nearly constant ($\sim r^{0.4}$) after $r\Delta z \approx 6$, which can serve as a choice of prefactor for the crossover length,

$$\ell^* \approx \frac{6}{\Delta z}. \tag{21}$$

For large r the relative fluctuations do not go to zero, which indicates that the system is not self-averaging. The length scale ℓ^* thus marks the distance at which the relative error stops growing. Note again that the r in this analysis refers to the distance from the perturbation where the fluctuations are measured and that the fluctuation analysis does not involve a coarse graining length. The fluctuations, at any r, are measured on the scale of single contacts. This contrasts with Sec. IV B, where we will relate ℓ^* to the coarse graining length needed to obtain a smooth response.

B. Inhomogeneity of global response

The results for the crossover length suggest that to obtain a smooth stress response field by coarse graining Δf, one would need to use a coarse graining length proportional to ℓ^*. To test this explicitly, we now study the stress fluctuations in packings under an overall shear as a function of the coarse graining length ξ_{CG}.

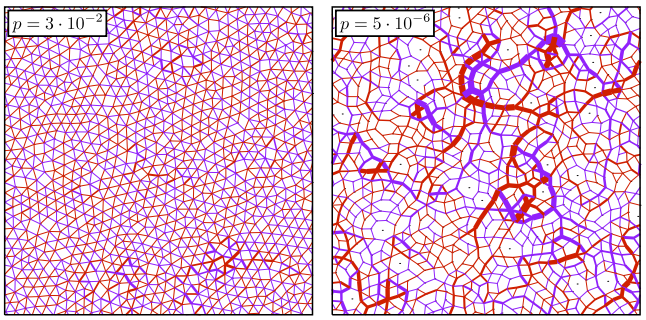

FIG. 9. (Color online) Force response networks for a global shear deformation of packings of 1000 particles at high (left) and low (right) pressures. The thickness of the border around the panel corresponds to a change in force of 0.5 (left) and 80 (right) per unit strain, respectively, which is needed because the shear modulus is much lower at the lower pressure. Note that in the high pressure case nearly all bonds that have an angle between 0 and $\pi/2$ with the x axis are red (decreased force) and nearly all bonds in the other diagonal direction are blue (increased force), consistent with the observation that the displacement fields for this shear response are very close to affine (Fig. 11). The response network of the low pressure packing is much more disordered. Note that in the black and white print, the blue lines will show up darker than the red lines.

The starting point is force response networks for packings of 10 000 particles that we obtain in linear response to shear (Fig. 9). The behavior is consistent with what we observed for point forcing: the characteristic length scale of these force fluctuations appears to grow when approaching the jamming point. To quantify this, we calculate the change in shear stress $\Delta\sigma_{xy}$ in 64 points using Eq. (11) with a Gaussian coarse graining function. The (relative) standard deviation of the resulting 64 values is a measure of the inhomogeneity of the response,

$$\Xi(\xi_{CG}) = \frac{1}{\langle \Delta\sigma_{xy}\rangle}\sqrt{\langle(\Delta\sigma_{xy}(x_i) - \langle\Delta\sigma_{xy}\rangle)^2\rangle},$$

where the averages are taken over the 64 points within each separate packing. In Fig. 10 we plot $\Xi(\xi_{CG})$ and obtain the inhomogeneities decay as $1/\xi_{CG}$. The force fluctuations thus lack an intrinsic length scale. We can however collapse the

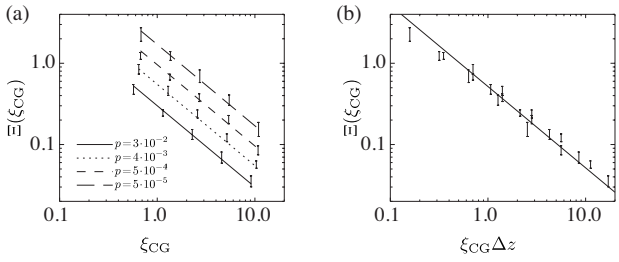

FIG. 10. (a) Inhomogeneity Ξ of the response as a function of coarse graining length ξ_{CG} for various pressures. The lines indicate the $1/\xi_{CG}$ behavior and the error bars denote the 20% median values of our data set of 90 packings at each pressure. (b) The same data with the horizontal axis rescaled by Δz to collapse the data. The line again denotes $\Xi \sim (\xi_{CG}\Delta z)^{-1}$.

data for Ξ for different pressures when they are plotted as a function of $\xi_{CG}\Delta z$. Therefore, the length scale $\ell^* \sim 1/\Delta z$, which was observed in the inflation response in Sec. IV A, can also be used to set the coarse graining length one needs to obtain a stress field with a particular inhomogeneity Ξ. It should be noted that Fig. 10 also implies that, for a fixed coarse graining length, the ensemble size one would need to obtain a desired smoothness of response grows as $(\Delta z)^{-2}$.

V. ENERGY MINIMIZATION AND LOCAL SLIDING

In this section we will explore various connections between the local displacement field, global energy minimization, and the scaling of the elastic moduli. In Sec. V A we present simple scaling arguments for the typical magnitude of $u_\perp$, $u_\parallel$ and their ratio as a function of the distance to the jamming point. In Sec. V B we employ the displacement angle distribution $P(\alpha)$ [8] to verify the latter scaling prediction and find that both under shear and under compression, the response of jammed packings becomes increasingly nonaffine near the jamming point. In Sec. V C we test the scaling predictions for the probability distributions $P(u_\parallel)$ and $P(u_\perp)$ and find that $u_\perp$ diverges near the jamming point, as predicted. However, while our simple scaling arguments capture the behavior of systems under shear in detail, they do not quantitatively capture the scaling of $P(u_\parallel)$ and $P(u_\perp)$ for jammed packings under compression.

A. Simple scaling arguments

We now present a set of simple scaling relations connecting the local displacement field to the scaling of the elastic moduli and global energy minimization. The starting point for our discussion is the energy expansion [Eq. (4)], which is a function of the relative displacements of particles in contact and which for our power law interparticle potential reads [56]

$$\Delta E = \frac{1}{2}\sum_{\langle i,j\rangle} k_{ij}\left(u_{\parallel,ij}^2 - \frac{2}{3}\delta_{ij}u_{\perp,ij}^2\right). \tag{22}$$

As explained in Sec. II B, k_{ij} is the stiffness d^2V_{ij}/dr_{ij}^2, where V_{ij} denotes the interparticle potential, δ_{ij} is the dimensionless overlap $1-r_{ij}/(R_i+R_j)$, and $u_\parallel(u_\perp)$ denotes the parallel (perpendicular) component of the relative displacement $\mathbf{u}_{ij}$ with respect to the vector $\mathbf{r}_{ij}$ connecting the centers of the contacting particles.

For the response to a global shear or compression, ΔE is also related to the elastic moduli through

$$\Delta E \sim C\epsilon^2 \sim \frac{1}{2}\sum_{\langle i,j\rangle} k_{ij}\left(u_{\parallel,ij}^2 - \frac{2}{3}\delta_{ij}u_{\perp,ij}^2\right), \tag{23}$$

where C refers to G and K for shear and compressive deformations, respectively, and ϵ is the applied strain. Note that the first term between brackets is strictly positive and the second term is strictly negative. Because the packings were constructed to be at an energy minimum, this implies that the second term cannot dominate over the first one and hence the scaling of typical values of $u_\parallel$ is connected to that of the corresponding modulus. Inserting $K/k \sim \delta^0$ and $G/k \sim \delta^{1/2}$ [3], we obtain

$$u_\parallel \sim \epsilon\delta^{1/4} \quad \text{for shear}, \tag{24}$$

$$u_\parallel \sim \epsilon\delta^0 \quad \text{for compression}, \tag{25}$$

where symbols without ij indices refer to typical or average values of the respective quantities. Note that by dividing out the stiffness k we obtained exponents that are valid for both harmonic and Hertzian interactions and in fact should be valid for all potentials of the form $V \sim \delta_{ij}^\alpha$.

The expected scaling for $u_\perp$, the amount by which particles in contact slide past each other, is more subtle. Because of the negative prefactor in Eq. (22), energy minimization should maximize these $u_\perp$. Again, they are bounded by the fact that these packings are stable: $u_{\parallel,ij}$ and $u_{\perp,ij}$ are not the independent variables of the problem, as they are coupled through the packing geometry, and for stable packings the question really is how close to the typical $u_\parallel^2$ the typical $\delta u_\perp^2$ can get. The best the system could do in order to minimize the change in energy is to make them of the same order, which suggests that

$$\frac{u_\parallel}{u_\perp} \sim \sqrt{\delta}. \tag{26}$$

In particular, this means that the system is always close to a buckling instability, so that compressing it would inevitably lead to the formation of more contacts to restabilize the system [7]. For the displacements in low energy eigenmodes, Eq. (26) has recently been derived [43]—more intuitively Eq. (26) can be understood as arising from the elastic distortion of floppy modes on a scale $\ell^* \sim 1/\Delta z \sim 1/\sqrt{\delta}$ [31]. Generically, one may expect this property to carry over to the displacements in response to external perturbations, but this is by no means guaranteed. Indeed, we shall find that Eq. (26) and the corresponding predictions for the scaling of $u_\perp$ break down in case of a global compression, while they work very well for the shear response. In a related paper, we studied this issue in depth in the context of networks of harmonic springs [31].

It is important to understand the relation between Eq. (22) and the excess coordination number $\Delta z = z - z_{iso}$. First, note that for $z < z_{iso}$, deformation fields exist for which $\Delta E = 0$—the so-called floppy modes (see Appendix C). Generically, right at the jamming transition ($z = z_{iso}$), there are just enough degrees of freedom to set all individual $u_{\parallel,ij}$ equal to zero for the type of response considered, in other words, to have sideways sliding motion for all of the bonds at jamming. For hyperstatic packings with $z > z_{iso}$, the $u_\parallel$ cannot all be set to zero anymore because there are more of them than the number of degrees of freedom dN. In addition, the Nd-dimensional coordinates are sufficiently constrained so that displacements which make the negative terms in ΔE outbalance the positive ones are forbidden and $\Delta E > 0$.

A thorough analysis of Eq. (26) involves the scaling of the distribution of the ratios $u_{\parallel,ij}/u_{\perp,ij}$ since the average of $u_\perp$ and $u_\parallel$ over all contacts may be dominated by large and rare fluctuations. To quantify the relative amount of sliding and

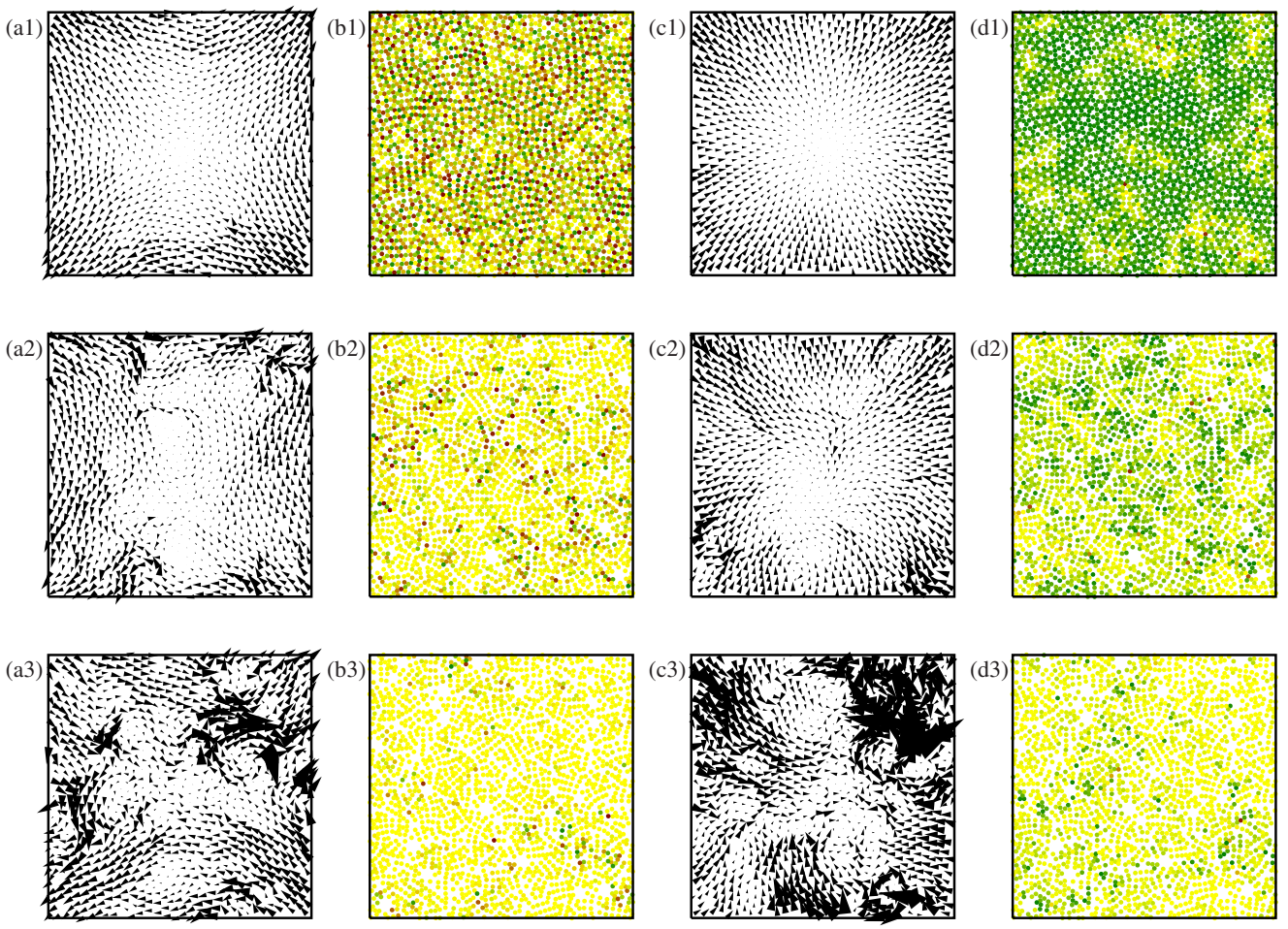

FIG. 11. (Color online) Examples of displacement fields in linear response to (a) shear and (c) compression for three pressures, $p=3\times10^{-2}$, 5×10^{-4}, 5×10^{-6}, from top to bottom. In (b) and (d) the corresponding displacement angles are depicted, where bonds are marked with a dot on a color scale which runs from red ($\alpha=0$), via bright yellow ($\alpha=\pi/2$), to green ($\alpha=\pi$)—see Eq. (27) for the definition of α. Clearly, the highest pressure packing displays almost affine displacements, while at lower pressures the response becomes increasingly nonaffine.

deformation, we therefore introduce the displacement angle α_{ij}, defined as the angle between $\mathbf{u}_{ij}$ and $\mathbf{r}_{ij}$ or

$$\tan\alpha_{ij}=\frac{u_{\perp,ij}}{u_{\parallel,ij}}. \tag{27}$$

In Sec. V B below we will present the probability densities $P(\alpha)$ for shear and compressive deformations as a function of the distance to point J and test the prediction given by Eq. (26) in detail.

In Sec. V C we will study the scaling of the distributions of $u_\parallel$ to test the predictions of Eqs. (24) and (25). We will also present the distributions of $u_\perp$ under shear and compression and explore to what extent these saturate the stability bound given by $u_\perp\sim u_\parallel/\sqrt{\delta}$. As alluded before, we will show that for the response to shear, $u_\perp$ follows the prediction from combining Eqs. (24) and (26), namely,

$$u_\perp\sim\epsilon\delta^{-1/4} \quad \text{for shear}. \tag{28}$$

The corresponding scaling for the response to compression would be, from Eqs. (25) and (26),

$$u_\perp\sim\epsilon\delta^{-1/2} \quad \text{for compression}, \tag{29}$$

but we will show that the numerical results do not support this—in the case of compression the two terms in the expansion of ΔE do not become of the same order.

Note that Eq. (26) predicts that the response of the system becomes strongly nonaffine near point J and that Eqs. (28) and (29) predict that typical distances by which particles slide past each other *diverge* as we approach the jamming transition. In finite systems, this divergence of the local displacements is limited by finite size effects. We discuss the corresponding finite size scaling and crossover in Appendix D.

B. Displacement field and displacement angle distribution

We extract the displacement fields from our linear response calculations of the periodic packings of 1000 particles. Examples of these, for both compression and shear and for three different pressures, are shown in Figs. 11(a) and 11(c) and the corresponding displacement angles α are shown in Figs. 11(b) and 11(d).

For high pressure, far from point J, the displacement fields are quite smooth and close to affine deformations, i.e., $\mathbf{u}=\epsilon(y\hat{\mathbf{x}}+x\hat{\mathbf{y}})$ for shear and $\mathbf{u}=-\epsilon(x\hat{\mathbf{x}}+y\hat{\mathbf{y}})$ for compression. When point J is approached, the displacement fields clearly become more disordered. The displacements become increasingly nonaffine and organize in vortexlike structures. Similar structures have been observed in various experimental and numerical studies of disordered systems close to the jamming transition [32,35,44–48].

In principle, this nonaffine behavior can be analyzed by subtracting the appropriate affine displacement field from the observed displacement field [33,46,47]. By doing so, however, valuable information on the correlation between $\mathbf{r}_{ij}$ and $\mathbf{u}_{ij}$ is lost. Therefore, we analyze the nature of the nonaffinity in terms of the displacement angles (α), where α is defined via $\tan\alpha_{ij}=u_{\perp,ij}/u_{\parallel,ij}$ [see Eq. (27)]. Under an affine compression, all particles get closer together along their contact line and $P(\alpha)$ would be a δ peak at $\alpha=\pi$. For a purely affine shear displacement field in an isotropic system, $P(\alpha)$ is flat [57]. Finally, close to point J where $\delta\to 0$, Eq. (26) predicts that $u_{\perp,ij}/u_{\parallel,ij}$ diverges, i.e., that $P(\alpha)$ approaches a δ peak at $\alpha=\pi/2$ (see also Appendix D).

The values of α in Figs. 11b1 and 11d1 are what one would expect for an affine displacement. One sees that close to jamming, more and more bonds have α close to $\pi/2$ (corresponding to the bright yellow dots in Figs. 11b2 and 11d2 and in particular Figs. 11b3 and 11d3), indicating that for those displacement fields $u_{\parallel}\ll u_{\perp}$, as predicted in Eq. (26).

For the rest of the paper we will ignore the spatial organization of the displacement angles α and focus on their probability densities $P(\alpha)$. In Fig. 12 we show these probability distributions for compressional and shear deformations for a range of pressures. For large pressures, $P(\alpha)$ reflects the affine limits discussed above, while upon lowering the pressure, $P(\alpha)$ evolves to exhibit a strong peak at $\alpha=\pi/2$, as predicted by Eq. (26). In the case of the shear deformation, we find that the peak in $P(\alpha)$ can be well approximated by a Lorentzian, and we fit $P(\alpha)$ to [58]

$$P(\alpha)\simeq\frac{1}{\pi w}\frac{1}{1+\left(\frac{\alpha-\pi/2}{w}\right)^2}. \tag{30}$$

Note that the width w should vary as $u_{\parallel}/u_{\perp}$ close to the jamming transition because $|\alpha_{ij}-\pi/2|\approx u_{\parallel,ij}/u_{\perp,ij}$ if $u_{\parallel,ij}\ll u_{\perp,ij}$.

In good approximation, the resulting widths satisfy the scaling relation

$$w\sim\delta^{0.55\pm0.05}, \tag{31}$$

as is shown in the inset of Fig. 12(a). This scaling has been used to construct the colored surface in Fig. 12(a) from Eq. (30) and is consistent with the prediction of Eq. (26), $w\sim\sqrt{\delta}$.

For the case of compression the situation is more complex as can be seen from Fig. 12(b). Since the distribution here does not appear to be governed by a single scale and we do not have a fitting function, we have used the full width at half maximum of $P(\alpha)$ as w. The value of this width is shown in the inset of Fig. 12(b). It scales as $w\sim\delta^{0.44}$[5], which is reasonably consistent with Eq. (26). However, the presence of a clear shoulder for $\alpha\simeq\pi$ is a strong indication that a simple one-parameter scaling actually does not hold [31].

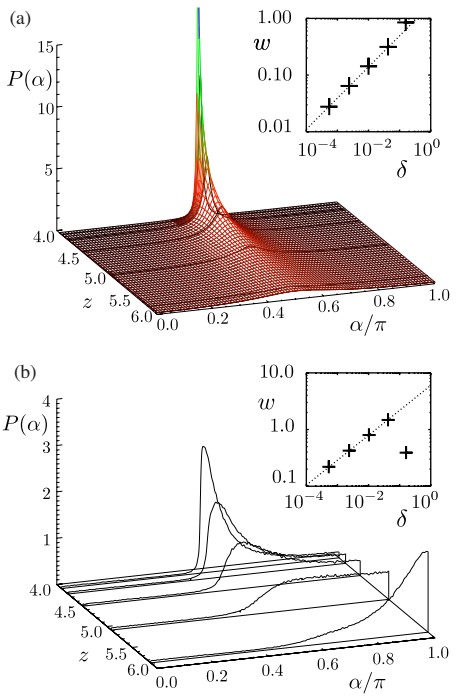

FIG. 12. (Color online) The displacement angle distribution for various pressures, obtained by averaging over 100 packings for each pressure. (a) Under shear $P(\alpha)$ evolves from nearly flat (highest pressure) to very sharply peaked at $\alpha=\pi/2$ (lowest pressure). The solid lines represent numerical data, the gridded surface [Eq. (30)]. Inset: the scaling of the width of the peak as a function of typical overlap δ. The dashed line indicates $w\sim\delta^{0.55}$. (b) Under compression $P(\alpha)$ has a peak at π for high pressures and develops a peak at $\pi/2$ at low pressures. Inset: the scaling of the width of the peak as a function of typical overlap δ. The dashed line indicates $w\sim\delta^{0.44}$.

The shear data shown in Fig. 12 are thus in agreement with the prediction from the simple scaling argument that near point J, $u_{\parallel}/u_{\perp}\sim\sqrt{\delta}$ [Eq. (26)]. Hence, we conclude that the displacements in response to shear do lead to an approximate balance between the two terms in ΔE [Eq. (22)]. The closer one gets to point J, the more strongly nonaffine the deformation field becomes, in other words, the more the mechanical response of the system is different from that of a homogeneous isotropic elastic material. For compressive deformations, the situation is somewhat more complicated: the development of a peak at $\alpha\approx\pi/2$ still signifies the same tendency to nonaffine sideways sliding motion with an amplitude that might be described by a balance of the two terms in the energy expression, but the remainder of a significant shoulder at large angles α hints at the fact that the response cannot be understood completely in terms of this balance or a simple one-parameter scaling. For more details, see Ref. [31].

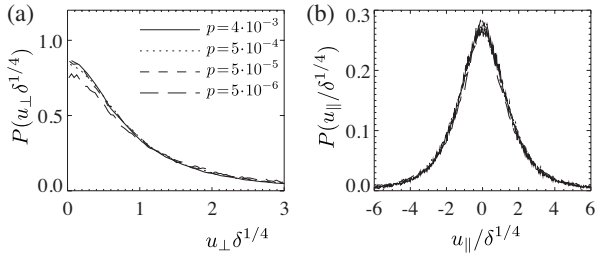

FIG. 13. Collapse of the probability densities of (a) $u_\perp$ and (b) $u_\parallel$ for a shear deformation. The axes have been rescaled according to the prediction of Eqs. (24) and (28). Higher pressures have been omitted from the analysis.

C. Scaling of local displacements

As we discussed in the introduction to this section, by linking the scalings of the local relative displacements to the elastic moduli, we can predict scaling relations for $u_\parallel$ and, when the two terms in the energy expansion are of the same order, for $u_\perp$, both for compressive and shear deformations. We now test these predictions by plotting the distributions of the rescaled displacements $P(u_\parallel\delta^{n_\parallel})$ and $P(u_\perp\delta^{n_\perp})$, where the power law indices n follow from Eqs. (24), (25), (28), and (29) and check for data collapse.

The appropriately rescaled distributions of $u_\parallel$ and $u_\perp$ are shown in Fig. 13 for the case of shear deformations. Note that we normalize the displacements by the strain ϵ [59]. As is clear from Fig. 13, the scaling collapse is very good for both components of the displacement field $\mathbf{u}_{ij}$, fully confirming the simple prediction for $u_\parallel$ presented in Eq. (24) and the prediction for $u_\perp$ in Eq. (28) that follows from the assumption that the two terms in the energy expansion are of the same order.

For the displacements under compression we show scaling collapses in Fig. 14 [60]. In Figs. 14(a) and 14(b) we show the distributions $P(u_\perp\delta^{0.5})$ and $P(u_\parallel\delta^0)$, which Eqs. (25) and (29) predict to collapse. Clearly, the collapse is far worse than in the case of jammed packings under shear. Similar to $P(\alpha)$, the distributions $P(u_\perp)$ and $P(u_\parallel)$ do not appear to exhibit simple scaling for jammed packings responding to compression. The best scaling collapse is obtained by adjusting the scaling exponents n by hand, but even then, Figs. 14(c) and 14(d) show that this adjusted scaling collapse is still less convincing than for systems under shear. The exponent $n_\perp=0.30$ is significantly different from the predicted value of 0.5, reflecting that the displacements in response to compression satisfy neither a balance of terms in the energy expansion nor pure one-parameter scaling [31].

In conclusion, the displacement angle distribution shows the development of a peak in $P(\alpha)$ at $\alpha=\pi/2$ both for shear and compressive deformations. The width of the peak shrinks as $\sqrt{\delta}$, consistent with the energy balance argument that predicts that $u_\parallel/u_\perp\sqrt{\delta}$. This peak signals that near point J, most particles in contact mainly slide past each other in a manner which helps to minimize the changes in elastic energy. However, in the case of compression $P(\alpha)$ retains a significant shoulder close to $\alpha=\pi$ even close to the jamming transition.

Both for shear and compressive deformations, the sliding motion $u_\perp$ diverges near jamming. This suggests that corrections due to finite size play a role—for details see Appendix D. For shear deformations, simple arguments predict the scaling of $P(u_\parallel)$ and $P(u_\perp)$ quantitatively correct, but for compressive deformations our simple arguments break down. We believe that this fact can ultimately be traced back to the special geometry that the contact network of a packing has because it is made of particles that interact purely repulsively. We have recently studied this question in the context of harmonic networks—for more information see Ref. [31].

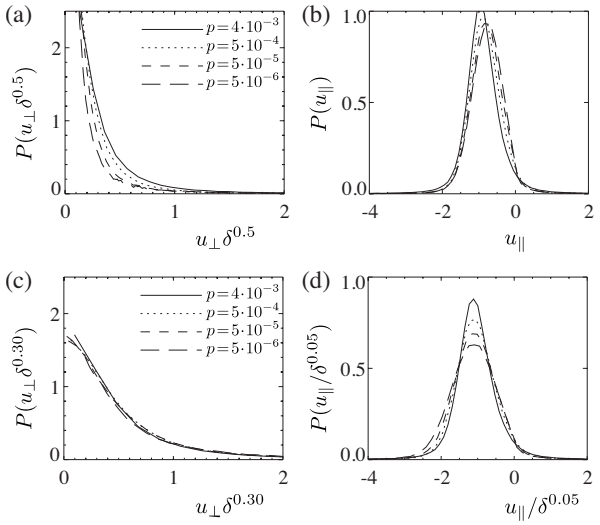

FIG. 14. Rescaled probability distributions of $u_\perp$ and $u_\parallel$ for compressional deformations. (a) and (b) Rescaling of $P(u_\perp)$ and $P(u_\parallel)$ with the exponents predicted by Eqs. (25) and (29) produces a poor collapse, indicative of the special nature of compression of jammed packings. (c) and (d) When the scaling exponents are adjusted by hand (c) from 0.5 to 0.3 and (d) from 0 to 0.05, a reasonable collapse can be obtained. As before, in all panels the distributions for the highest pressure have been omitted.

VI. SUMMARY AND OUTLOOK

We have shown, by means of linear response calculations, how the applicability of elasticity theory to disordered packings of frictionless spheres is related to the distance to the jamming transition. Averaging the response to a local perturbation over an ensemble of packings, we fitted the stress response to continuum elasticity. The resulting elastic moduli are the same as those obtained by calculating the response to a global shear or compression, proving the consistent applicability of continuum elasticity in an ensemble averaged sense. In *single packings*, we identified a length scale $\ell^*\sim1/(\Delta z)$ up to which the response is dominated by local disorder. Since ℓ^* diverges as the jamming transition is approached, continuum elasticity breaks down completely as a description of the linear response of individual packings near jamming. The length scale ℓ^* corresponds to the length used by Wyart *et al.* to estimate the number of soft modes in systems near jamming [6]. Here we have shown that it also represents the coarse graining length needed to obtain a smooth stress response tensor in a single globally deformed packing.

The displacement fields near jamming are highly nonaffine. We analyzed these displacements at the grain scale through the statistics of local relative displacements of neighboring particles. These relative displacements, decomposed into $u_\parallel$ along the line of contact and $u_\perp$ perpendicular to it, govern the elastic behavior of the system because according to Eq. (4) they enter into the change in energy as

$$\Delta E = \frac{1}{2}\sum_{\langle i,j\rangle} k_{ij}\left(u_{\parallel,ij}^2 - \frac{f_{ij}}{k_{ij}r_{ij}}u_{\perp,ij}^2\right).$$

We have introduced the displacement angle distribution $P(\alpha)$ to easily characterize the nonaffinities via the angle between the relative displacement vector and the vector connecting two neighboring particles. Close to point J, these distributions develop a peak near $\alpha=\pi/2$, indicating that the nonaffinity is such that particles predominantly slide past each other.

We also determined the scaling of typical values of $u_\perp$ and $u_\parallel$ separately. The parallel displacements $u_\parallel$ follow a scaling that is consistent with the scaling of the elastic moduli: they are nearly independent of distance to jamming for compression and vanish as $\delta^{1/4}$ for shear. The perpendicular displacements $u_\perp$ diverge in response to both shear and compression, consistent with the predominance of sliding near jamming.

There is a surprising and fundamental difference between compression and shear. For shear, $u_\perp$ simply scales as $\delta^{-1/4}$, so that both terms in the elastic energy are of the same order, and the scaling of $P(\alpha)$ is captured by a single parameter. For bulk compression, all of this breaks down—$u_\perp$ still diverges but not with an exponent that follows from a simple scaling argument, and there is no one-parameter scaling for $P(\alpha)$. The issue of what is special about the compression of packings is discussed in a separate paper [31].

There are many extensions of this framework beyond the linear response of frictionless disks in a computer simulation, of which the extension to three-dimensional spheres is probably the simplest. For finite displacements, the direct connection between displacements and energy is lost. However, in any system of approximately spherical particles close to the jamming transition, where steric hindrance becomes an important factor in the dynamics, one would expect the displacement angle distribution to develop a maximum near $\alpha=\pi/2$, corresponding to predominantly sliding displacements. These local displacement statistics are accessible experimentally even outside the linear response regime, for example, in steadily sheared (wet) foams or emulsions and even in systems below the jamming density, for example, in driven granular gases [49–52]. In the latter case, one has to define neighbors (e.g., through a Voronoi tesselation), and one has to choose the time scale τ over which to measure the relative displacements so that neighboring particles have had the time to interact—$P(\alpha)$ will depend on τ, and preliminary studies suggest that the peak in $P(\alpha)$ is maximal for a finite value of τ. Note that in dense foams or emulsions, in which the particles are continuously interacting, one rather expects the peak of $P(\alpha)$ to be maximal for $\tau\to 0$.

In systems of ellipsoids [15–18] or frictional particles [12,13], rotations and torques come into play, and the expression for the elastic energy will be more complicated than Eq. (4). However, in linear response the elastic energy will still be a function of the local relative changes of the particle coordinates, and one can still check for the occurrence of combinations of local displacements that lead to a small or vanishing change in energy. For example, in packings of frictional spheres, the locally floppy displacement is for contacting particles to roll without slipping. For ellipses "zero energy" local displacements can be identified similarly. We expect that such low energy displacements should dominate the statistics when the system is close to the relevant isostatic limit, and we expect that appropriate generalizations of $P(\alpha)$ for such systems may serve as a useful characterization of the nonaffine deformation field.

ACKNOWLEDGMENTS

We thank E. Somfai for providing the numerical code to construct the granular packings and for many crucial discussions. In addition, we are grateful to M. Wyart for several discussions that have been very enlightening and helpful. We wish to thank N. Xu, K. Shundyak, J. H. Snoeijer, M. Depken, C. Goldenberg, S. Ostojic, S. R. Nagel, A. J. Liu, Z. Zeravcic, and H. van der Vorst for useful discussions and suggestions. W.G.E. acknowledges support from the Stichting voor Fundamenteel Onderzoek der Materie (FOM) and M.v.H. from the Dutch Science Foundation NWO through a VIDI grant. W.G.E. thanks the Aspen Center for Physics, where part of this work was done, for its hospitality.

APPENDIX A: PACKING GENERATION

Hertzian interaction

The Hertzian interaction is taken from Refs. [32,36] in terms of a *force law* as

$$f_{ij} = \frac{4}{3}\sqrt{R_{ij}}E_{ij}^*(R_i + R_j - r_{ij})^{3/2}, \tag{A1}$$

where R_{ij} is the reduced radius of the pair of particles defined by

$$\frac{1}{R_{ij}} = \frac{1}{R_i} + \frac{1}{R_j}$$

and E_{ij}^* is a similar combination of the modified Young moduli,

$$\frac{1}{E_{ij}^*} = \frac{1}{E_i^*} + \frac{1}{E_j^*}.$$

The modified Young modulus is determined from the Young modulus E and the Poisson ratio ν of the material that the grains are made of,

$$E^* = \frac{E}{1-\nu^2}.$$

Now let us determine a closed expression for the prefactor ϵ_{ij} of the interaction as we have used it throughout the paper.

Differentiating the interaction in Eq. (1) gives

$$f_{ij} = \frac{5}{2}\frac{\epsilon_{ij}}{d_{ij}}\left(1 - \frac{r_{ij}}{d_{ij}}\right)^{3/2}, \tag{A2}$$

with $d_{ij}=R_i+R_j$. Equating Eqs. (A1) and (A2) yields

$$\epsilon_{ij} = \frac{8}{15}\sqrt{R_{ij}}E^*_{ij}d^{5/2}_{ij}.$$

Our unit of pressure is E^*_i (and all grains are made from the same material), so that in our reduced units $E^*_{ij}=\frac{1}{2}$ and

$$\epsilon_{ij} = \frac{4}{15}\sqrt{R_{ij}}d^{5/2}_{ij}. \tag{A3}$$

With the radii of the particles drawn from a flat distribution between $0.4 \le R_i \le 0.6$, the value of ϵ_{ij} can vary between 0.068 and 0.230. To check how large the effect of this varying ϵ is, we have performed some simulations using a constant $\epsilon=\frac{2}{15}$, the value it has for $R=0.5$, and did not observe significant deviations. This justifies comparing our results to other simulations done at constant ϵ [3].

APPENDIX B: 2D ELASTICITY AND POINT RESPONSE

The two-dimensional version of linear elasticity has the same form for Hooke's law as the well-known 3D version [40,53],

$$\sigma_{\alpha\beta} = 2\mu u_{\alpha\beta} + \lambda u_{\xi\xi}\delta_{\alpha\beta},$$

where $u_{\alpha\beta}$ is the strain tensor, $\delta_{\alpha\beta}$ is the Kronecker delta, and we use the summation convention. λ and μ are known as the Lamé coefficients. All dependence on dimensionality basically arises from the $\delta_{\alpha\beta}$ through the fact that the trace of $\sigma_{\alpha\beta}$ reads

$$\sigma_{\alpha\alpha} = (2\mu + d\lambda)u_{\alpha\alpha}.$$

The shear modulus G is just the same as the Lamé coefficient μ, independent of d. The definition of the bulk modulus K is the resistance to change of "volume,"

$$K = -\frac{p}{V/V_0}.$$

In an isotropic material the stress tensor corresponding to a uniform compression is $\sigma_{\alpha\beta}=p\delta_{\alpha\beta}$. Its trace is therefore $\sigma_{\alpha\alpha}=pd$. The trace of the strain tensor is $u_{\alpha\alpha}=V/V_0$, so that in $d=2$, we now have for the moduli

$$G = \mu, \tag{B1}$$

$$K = \frac{\sigma_{\alpha\alpha}}{du_{\alpha\alpha}} = \lambda + \frac{2}{d}\mu = \lambda + \mu. \tag{B2}$$

The Navier-Cauchy equation, which follows from inserting Hooke's law and the definition of the strain tensor into the equation of mechanical equilibrium $\partial_\beta\sigma_{\alpha\beta}=-f^{\text{ext}}_\alpha$, reads (in arbitrary dimension),

$$\mu\Delta\mathbf{u} + (\lambda + \mu)\nabla(\nabla\cdot\mathbf{u}) = -\mathbf{f}^{\text{ext}},$$

where Δ denotes the Laplacian operator. In $d=2$ the coefficients happen to become simply

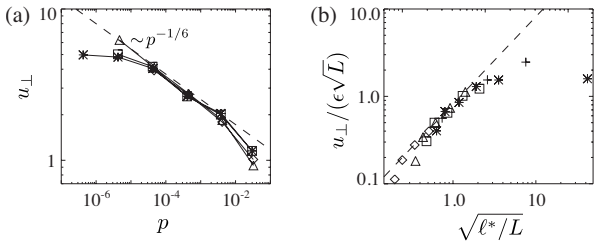

FIG. 15. (a) Scaling of typical $u_\perp$ under shear with pressure p. The dashed line indicates $u_\perp \sim p^{-1/6}$, to which all large packings stay close except for the bottom-right points which are very far from point J ($p=3\times10^{-2}$). The system size decreases from $N=10\,000$ (diamonds), $N=1000$ (triangles), $N=300$ (squares) to $N=100$ (stars). The curve seems to level off at small p for the small systems, as predicted in Eq. (D3). (b) The same data plotted according to the finite size scaling prediction of Eq. (D7). The plus signs indicate data taken from the linear response to shear of bidisperse packings generated using conjugate gradient minimization (courtesy of Xu), which allows us to probe much lower pressures. The two rightmost points in this graph represent series of packings which are essentially isostatic and hence have a very large and inaccurate ℓ^*. The dashed line represents the predicted behavior for small ℓ^*/L.

$$G\Delta\mathbf{u} + K\nabla(\nabla\cdot\mathbf{u}) = -\mathbf{f}^{\text{ext}}, \tag{B3}$$

which is Eq. (14).

Response to a point force

For a rectangular packing with periodic x boundaries and hard walls on top and bottom, the Navier-Cauchy equation [Eq. (B3)] can be solved in terms of a Fourier series. For a point force in the middle, taken to be the origin of the coordinate system, we expand

$$u_x = \sum_{lm} A_{lm}\sin\left(\frac{2\pi lx}{L_x}\right)\sin\left(\frac{\pi my}{L_y}\right), \tag{B4}$$

$$u_y = \sum_{lm} B_{lm}\cos\left(\frac{2\pi lx}{L_x}\right)\cos\left(\frac{\pi my}{L_y}\right), \tag{B5}$$

$$f_x = 0, \tag{B6}$$

$$f_y = \sum_{lm} F_{lm}\cos\left(\frac{2\pi lx}{L_x}\right)\cos\left(\frac{\pi my}{L_y}\right), \tag{B7}$$

where

$$F_{lm} = \begin{cases} \dfrac{2}{L_xL_y}, & m \text{ odd}, \\ 0, & m \text{ even}, \end{cases} \tag{B8}$$

so f_y represents a δ force in the origin of unit weight. The solution is to be compared to granular stress fields which have been coarse grained using a Gaussian. Using the same Gaussian instead of a δ function for f_y here leads to a better fit and to improved convergence of the resulting Fourier series for the stress tensor. Since convolution in real space is

just multiplication in Fourier space this amounts to multiplying F_{lm} by

$$\frac{2}{L_x L_y}\exp\left[-\pi^2\sigma^2\left(\frac{2l^2}{L_x^2}-\frac{m^2}{2L_y^2}\right)\right].$$

Inserting the expansions into Eq. (B3) we can solve for A_{lm} and B_{lm}. Solutions for the strain tensor and stress tensor are then obtained by taking the appropriate linear combinations of derivatives of u_x and u_y. The resulting stress tensor only depends on the Poisson ratio $\nu=(K-G)/(K+G)$. A separate fitting procedure for the displacement field then gives $K+G$ using Eq. (16) and the determination of the moduli is complete.

APPENDIX C: FLOPPY MODES

Suppose we are at point J, so $\delta=0$, $z=4$, and the number of contacts equals $2N$, which is equal to the number of independent displacement components $u_{i,\alpha}$. When one contact is removed, we can in principle write down a displacement field for which all $u_{\parallel,ij}=0$. This displacement field has energy zero: it is a *floppy mode* [6,37]. This is not merely an artifact of the expansion in $u_\parallel$ and $u_\perp$: the counting of variables and equations in principle allows us to write down a displacement field for which the unexpanded Δr_{ij} from Eq. (3) is zero and hence the change in energy is strictly zero. For a floppy mode distortion, ΔE is identically zero to all orders in the distortion even if the initial configuration did not obey force balance. Let us check this up to $\mathcal{O}(u_\perp^4)$ in the expansion of ΔE. To see this, we include the term linear in $u_\parallel$, which we left out of original Eq. (4) because it vanishes when summed over all contacts,

$$\Delta E=\sum_{\langle i,j\rangle}\left[-f_{ij}u_{\parallel,ij}+\frac{1}{2}k_{ij}\left(u_{\parallel,ij}^2-\frac{f_{ij}}{k_{ij}r_{ij}}u_{\perp,ij}^2\right)\right].$$

For a floppy mode, $\Delta r_{ij}=0$, and this implies that $u_{\parallel,ij}=-u_{\perp,ij}^2/(2r_{ij})+\mathcal{O}(u_\perp^4)$. Hence, the first and third terms in the expansion of ΔE cancel without having to sum over all contacts and we are left with $\Delta E=\mathcal{O}(u_\perp^4)$. This even holds if the initial system would not satisfy force balance [61].

APPENDIX D: FINITE SIZE EFFECTS

If the system is sheared or compressed, local relative displacements diverge upon approaching the jamming point, according to the analysis in Sec. V C. However, the relative displacement between a given particle i and its image in the neighboring unit cell of the periodic packing is given by the imposed boundary condition—hence there is coupling between the magnitude of the local relative displacements and the system size. In addition, we have extracted the length scale ℓ^* from the elastic behavior of our system and should consider what happens when this length scale becomes of the order of the system size. We tentatively suggest the following picture for the implications of this coupling.

Let us focus on shear deformations because the scalings are cleanest in that case. The x component of the relative displacement between a particle at (x_i,y_i) and its periodic image at (x_i,y_i+L) can be written as a sum along a path from the particle to its image,

$$\sum_{\text{path}} u_{ij,x}=\epsilon L, \tag{D1}$$

where ϵ is the applied shear strain. If the system is small compared to the length scale ℓ^*, we do not expect to see any elastic behavior, and the displacement field is dominated by the local packing disorder. In this case, we might just as well view the displacements in the x direction as we go along the path as a random walk. This walk consists of approximately L steps of size roughly $u_\perp$, so that

$$\sum_{\text{path}} u_{ij,x}\sim u_\perp\sqrt{L}. \tag{D2}$$

Equating Eqs. (D1) and (D2) yields

$$u_\perp\sim\epsilon\sqrt{L}\quad\text{for } L\ll\ell^*. \tag{D3}$$

On the other hand, large systems can be treated as a continuum down to the scale ℓ^*, so if we want to apply this model to a large system, we have to consider the "random walk" in a subsystem of size ℓ^* and assume that the globally applied shear deformation scales down affinely to that scale. Therefore the boundary condition becomes

$$\sum_{\text{subsystem}} u_{ij,x}=\epsilon\ell^* \tag{D4}$$

and the random walk in the subsystem gives

$$\sum_{\text{subsystem}} u_{ij,x}\sim u_\perp\sqrt{\ell^*}, \tag{D5}$$

so that finally

$$u_\perp\sim\epsilon\sqrt{\ell^*}\quad\text{for } L\gg\ell^*. \tag{D6}$$

Hence the argument reproduces our result for the scaling of $u_\perp$ under shear [Eq. (28)] because $\ell^*\sim\delta^{-1/2}$. Furthermore, it predicts that $u_\perp$ should saturate around the value it has when $L=\ell^*$ when approaching the jamming transition in a finite system. The two limits can be connected by a finite size scaling function

$$u_\perp\approx\epsilon\sqrt{L}f\left(\sqrt{\frac{\ell^*}{L}}\right), \tag{D7}$$

where $f(x)\to\text{const}$ as $x\gg1$ and $f(x)\sim x$ as $x\ll1$. We do not have enough data on systems where $L\ll\ell^*$ to prove this scaling prediction with firm confidence, but the data we have are at least consistent with it. In Fig. 15, we show the typical values of $u_\perp$ as a function of p for various system sizes, taking $\ell^*=6/\Delta z$ in accord with Eq. (21). Figure 15(b) shows the scaling collapse corresponding to Eq. (D7). The two rightmost points in this plot have $z\approx4$, so ℓ^* is very large and very inaccurate, but nevertheless some leveling off of the curve can be observed. More data using packings between 100 and 1000 particles at $4.005\le z\le4.02$ could shed more light on the scaling behavior.

[1] A. J. Liu and S. R. Nagel, Nature (London) **396**, 21 (1998).
[2] V. Trappe, V. Prasad, L. Cipelletti, P. N. Segre, and D. A. Weitz, Nature (London) **411**, 772 (2001).
[3] C. S. O'Hern, L. E. Silbert, A. J. Liu, and S. R. Nagel, Phys. Rev. E **68**, 011306 (2003).
[4] L. E. Silbert, A. J. Liu, and S. R. Nagel, Phys. Rev. Lett. **95**, 098301 (2005).
[5] L. E. Silbert, A. J. Liu, and S. R. Nagel, Phys. Rev. E **73**, 041304 (2006).
[6] M. Wyart, S. R. Nagel, and T. A. Witten, Europhys. Lett. **72**, 486 (2005).
[7] M. Wyart, L. E. Silbert, S. R. Nagel, and T. A. Witten, Phys. Rev. E **72**, 051306 (2005).
[8] W. G. Ellenbroek, E. Somfai, M. van Hecke, and W. van Saarloos, Phys. Rev. Lett. **97**, 258001 (2006).
[9] F. Bolton and D. Weaire, Phys. Rev. Lett. **65**, 3449 (1990).
[10] D. J. Durian, Phys. Rev. E **55**, 1739 (1997).
[11] D. Weaire and S. Hutzler, *The Physics of Foams* (Oxford University Press, Oxford, 2001).
[12] H. A. Makse, N. Gland, D. L. Johnson, and L. M. Schwartz, Phys. Rev. Lett. **83**, 5070 (1999).
[13] E. Somfai, M. van Hecke, W. G. Ellenbroek, K. Shundyak, and W. van Saarloos, Phys. Rev. E **75**, 020301(R) (2007).
[14] K. Shundyak, M. van Hecke, and W. van Saarloos, Phys. Rev. E **75**, 010301(R) (2007).
[15] A. Donev, I. Cisse, D. Sachs, E. A. Variano, F. H. Stillinger, R. Connelly, S. Torquato, and P. M. Chaikin, Science **303**, 990 (2004).
[16] A. Wouterse, S. R. Williams, and A. P. Philipse, J. Phys.: Condens. Matter **19**, 406215 (2007).
[17] Z. Zeravcic, N. Xu, A. J. Liu, S. R. Nagel, and W. van Saarloos, EPL **87**, 26001 (2009).
[18] M. Mailman, C. F. Schreck, C. S. O'Hern, and B. Chakraborty, Phys. Rev. Lett. **102**, 255501 (2009).
[19] I. Goldhirsch and C. Goldenberg, Eur. Phys. J. E **9**, 245 (2002).
[20] C. Goldenberg and I. Goldhirsch, Phys. Rev. Lett. **89**, 084302 (2002).
[21] C. Goldenberg and I. Goldhirsch, Nature (London) **435**, 188 (2005).
[22] C. Goldenberg, A. P. F. Atman, P. Claudin, G. Combe, and I. Goldhirsch, Phys. Rev. Lett. **96**, 168001 (2006).
[23] L. Vanel, D. Howell, D. Clark, R. P. Behringer, and E. Clément, Phys. Rev. E **60**, R5040 (1999).
[24] D. Serero, G. Reydellet, P. Claudin, E. Clément, and D. Levine, Eur. Phys. J. E **6**, 169 (2001).
[25] J. Geng, D. Howell, E. Longhi, R. P. Behringer, G. Reydellet, L. Vanel, E. Clément, and S. Luding, Phys. Rev. Lett. **87**, 035506 (2001).
[26] G. Reydellet and E. Clément, Phys. Rev. Lett. **86**, 3308 (2001).
[27] M. Otto, J.-P. Bouchaud, P. Claudin, and J. E. S. Socolar, Phys. Rev. E **67**, 031302 (2003).
[28] A. P. F. Atman, P. Brunet, J. Geng, G. Reydellet, P. Claudin, R. P. Behringer, and E. Clément, Eur. Phys. J. E **17**, 93 (2005).
[29] S. Ostojic and D. Panja, Phys. Rev. Lett. **97**, 208001 (2006).
[30] H. A. Makse, N. Gland, D. L. Johnson, and L. M. Schwartz, Phys. Rev. E **70**, 061302 (2004).
[31] W. G. Ellenbroek, Z. Zeravcic, W. van Saarloos, and M. van Hecke, EPL **87**, 34004 (2009).
[32] E. Somfai, J.-N. Roux, J. H. Snoeijer, M. van Hecke, and W. van Saarloos, Phys. Rev. E **72**, 021301 (2005).
[33] F. Leonforte, A. Tanguy, J. P. Wittmer, and J.-L. Barrat, Phys. Rev. B **70**, 014203 (2004).
[34] W. G. Ellenbroek, E. Somfai, W. van Saarloos, and M. van Hecke, in *Powders and Grains 2005*, edited by R. García-Rojo, H. J. Herrmann, and S. McNamara (A. A. Balkema, Rotterdam, 2005), pp. 377–380.
[35] A. Tanguy, J. P. Wittmer, F. Leonforte, and J.-L. Barrat, Phys. Rev. B **66**, 174205 (2002).
[36] K. L. Johnson, *Contact Mechanics* (Cambridge University Press, Cambridge, 1985).
[37] S. Alexander, Phys. Rep. **296**, 65 (1998).
[38] R. Barrett, M. Berry, T. F. Chan, J. Demmel, J. Donato, J. Dongarra, V. Eijkhout, R. Pozo, C. Romine, and H. V. der Vorst, *Templates for the Solution of Linear Systems: Building Blocks for Iterative Methods* (SIAM, Philadelphia, PA, 1994).
[39] A. W. Lees and S. F. Edwards, J. Phys. C **5**, 1921 (1972).
[40] B. Lautrup, *Physics of Continuous Matter* (IOP, Bristol, 2005).
[41] M. Wyart, Ann. Phys. (Paris) **30** (3), 1 (2005).
[42] K. Walton, J. Mech. Phys. Solids **35**, 213 (1987).
[43] M. Wyart, H. Liang, A. Kabla, and L. Mahadevan, Phys. Rev. Lett. **101**, 215501 (2008).
[44] F. Radjai and S. Roux, Phys. Rev. Lett. **89**, 064302 (2002).
[45] A. Lemaître and C. Maloney, J. Stat. Phys. **123**, 415 (2006).
[46] A. Tanguy, F. Leonforte, J. P. Wittmer, and J. L. Barrat, Appl. Surf. Sci. **226**, 282 (2004).
[47] C. E. Maloney, Phys. Rev. Lett. **97**, 035503 (2006).
[48] D. L. Blair (private communication).
[49] A. R. Abate and D. J. Durian, Phys. Rev. E **74**, 031308 (2006).
[50] P. M. Reis, R. A. Ingale, and M. D. Shattuck, Phys. Rev. Lett. **98**, 188301 (2007).
[51] P. M. Reis, R. A. Ingale, and M. D. Shattuck, Phys. Rev. E **75**, 051311 (2007).
[52] A. S. Keys, A. R. Abate, S. C. Glotzer, and D. J. Durian, Nat. Phys. **3**, 260 (2007).
[53] L. D. Landau and E. M. Lifshitz, *Theory of Elasticity* (Pergamon Press, London, 1959).
[54] The point which deviates from the scaling of G is obtained for the lowest pressure from the point response. We believe this large deviation to be due to the fitting procedure: we fit the Poisson ratio ν from the stress field $\Delta\sigma_{\alpha\beta}(\mathbf{r})$. As $p\to 0$, we observe $\nu\to 1$, its maximum value in two dimensions. In this limit, the fitting of the stress tensor becomes less accurate for numerical reasons, which is made even worse by the fact that the data become more noisy at low p. In the bulk response we see a similar effect: the fluctuations around the average values are much larger at lower pressure.
[55] See page 21 in Ref. [53].
[56] For a general potential $V_{ij}\sim\delta_{ij}^{\alpha}$ the factor 2/3 in Eq. (22) becomes $1/(\alpha-1)$.
[57] This is easily seen in the case of a simple shear in the x direction: all $\mathbf{u}_i$ are in the x direction, hence so are the $\mathbf{u}_{ij}$, while the $\mathbf{r}_{ij}$ are isotropic.
[58] Because of the π-periodic nature of the angle α, we add copies of the peak at $-\pi/2$ and at $3\pi/2$. This improves the fit for larger pressures.
[59] In addition, it is natural to eliminate systematic dependence of $u_{\parallel}$ and $u_{\perp}$ on the particle radii, and we have divided each $u_{\perp,ij}$ and $u_{\parallel,ij}$ by the actual length r_{ij} of the contact—this would also

allow us to compare the results to the case of affine displacements, which have local $u_{\perp,ij}$ and $u_{\parallel,ij}$ which are proportional to r_{ij}, but we have already seen that the displacements are strongly nonaffine, so we do not show the corresponding plot here.

[60] Note that because the distribution of $u_{\parallel}$ under compression is not centered around zero, we are collapsing the average of the distributions, not the width.

[61] This holds in general for floppy modes in systems with radial interactions between the particles.